Nano Research 2017, 10(3): 767–775
DOI 10.1007/s12274-016-1289-1
Research Article
ISSN 1998-0124
CN 11-5974/O4

Real-time electrical detection of epidermal skin MoS_2 biosensor for point-of-care diagnostics

Geonwook Yoo[1,§], Heekyeong Park[2,§], Minjung Kim[2,§], Won Geun Song[2], Seokhwan Jeong[2], Min Hyung Kim[3], Hyungbeen Lee[3], Sang Woo Lee[3], Young Ki Hong[2], Min Goo Lee[4], Sungho Lee[4] (✉), and Sunkook Kim[2] (✉)

[1] *School of Electronic Engineering, Soongsil University, Seoul 06978, Republic of Korea*
[2] *Multi-Functional Nano/Bio Electronics Lab., Kyung Hee University, Gyeonggi 17104, Republic of Korea*
[3] *Department of Biomedical Engineering, Yonsei University, Wonju 26493, Republic of Korea*
[4] *Korea Electronics Technology Institute, Gyeonggi 13488, Republic of Korea*
[§] *These authors contributed equally to this work.*

Received: 14 June 2016
Revised: 18 August 2016
Accepted: 14 September 2016

KEYWORDS
epidermal skin biomarker,
MoS_2,
biosensor,
real-time,
point-of-care diagnostics

ABSTRACT

Various approaches have been proposed for point-of-care diagnostics, and in particular, optical detection is preferred because it is relatively simple and fast. At the same time, field-effect transistor (FET)-based biosensors have attracted great attention because they can provide highly sensitive and label-free detection. In this work, we present highly sensitive, epidermal skin-type point-of-care devices with system-level integration of flexible MoS_2 FET biosensors, read-out circuits, and light-emitting diode (LEDs) that enable real-time detection of prostate cancer antigens (PSA). Regardless of the physical forms or mechanical stress conditions, our proposed high-performance MoS_2 biosensors can detect a PSA concentration of 1 pg·mL^{-1} without specific surface treatment for anti-PSA immobilization on the MoS_2 surface on which we characterize and confirm physisorption of anti-PSA using Kelvin probe force microscopy (KPFM) and tapping-mode atomic force microscopy (tm-AFM). Furthermore, current modulation induced by the binding process was stably maintained for longer than 2–3 min. The results indicate that flexible MoS_2-based FET biosensors have great potential for point-of-care diagnostics for prostate cancer as well as other biomarkers.

1 Introduction

Prostate cancer, which grows slowly and initially shows no symptoms, is the most common cancer and leading cause of cancer-related death in males in the United States, and accounts for approximately 15% of all male cancer cases in developed countries and 4% in developing countries [1, 2]. Many studies recommend

Address correspondence to Sungho Lee, slee@keti.re.kr; Sunkook Kim, kimskcnt@gmail.com

that early detection can decrease prostate cancer mortality, and hence, various diagnostic methods have been used for cancer screening, e.g., prostate imaging using ultrasound and magnetic-resonance imaging, biopsies, and oncological markers [3–6]. Among these methods, the use of serum prostate-specific antigen (PSA) as a biomarker is most widely adopted because of its convenience and patient satisfaction, although the diagnosis is fully confirmed through a biopsy. Currently, most diagnoses are conducted at a special hospital with dedicated centralized laboratories, resulting in inconvenient clinical visits and high cost. With recent advances in biosensor-related technologies, point-of-care (POC) testing and active surveillance near patients has become a trend, and so portable diagnostic methods using PSA are widely investigated [7–9]. In addition, PSA detection is used for forensic determination in sexual assault cases, and so rapid and reliable testing at the crime sites is recommended [10, 11].

Various biosensor platforms have been proposed as promising POC tests for PSA, and field-effect transistor (FET)-based biosensors using electrochemical signal transduction have received much attention because of their simple, accurate, and cost-effective detection [8, 12]. FET biosensors are effective in determining binding events of charged or polar biological analytes through changes in the channel conductance, which is induced by the electrostatic interaction between the biomolecules and functionalized gate-dielectric or semiconductor channels, enabling highly sensitive detection of PSA [13, 14]. Furthermore, the development of nanomaterials or nanostructures including Si-nanowires (NWs) and single-walled carbon nanotube (SWNTs) as an integral part of the FET configuration offers significant merits over label-based optical detection methods in that they can eliminate sample preparation and labeling steps without sacrificing sensitivity [13, 15]. Despite its high sensitivity, however, biosensors based on one-dimensional (1-D) nanomaterials are not only prone to significant variation in performance due to the difficulty of controlling thickness, purity, and defects, but also lack a reliable fabrication process into transistors and integrated circuits [16, 17]. On the other hand, the conventional silicon-based FET biosensor can be integrated into complex device architectures; however, the structures must include functionalized and protective materials to be used in biological testing media, resulting in reduced sensitivity due to degraded electrochemical signal transduction [14]. Otherwise, oxide passivation itself is not sufficient to functionalize the surface because of the hydrophilic property, and thus the binding event becomes less efficient.

The recent advent of two-dimensional (2-D) nanomaterials, such as graphene and transition metal dichalcogenide (TMD), shows the possibility of an ultra-sensitive biosensor [18–21]. In particular, the existence of a bandgap in TMDs compared to zero-bandgap graphene and carrier transport modulation of 2-D layered materials by their surrounding net charges are critical for the FET-based platform, because the binding process at the interface between MoS_2 and biomolecules can induce a direct change of electrical properties including the threshold voltage (V_{TH}), field-effect mobility (μ_{eff}), and subthreshold swing (SS) [22, 23]. Therefore, the type or quantity of the charged biomolecules can be measured and correlated quantitatively. Recently, MoS_2-based biosensors using a hafnium oxide (HfO_2) gate dielectric layer with surface chemical treatment of 3-aminoproplytriethoysilane (APTES) have been demonstrated, and by adopting the hydrophobicity of the MoS_2 surface, our group reported the possibility of a PSA biosensor based on bottom-gated MoS_2 FETs with no additional surface treatment [20].

Here, we report a highly sensitive flexible biochip with system-level integration of a MoS_2 FET biosensor, read-out circuit, and a light-emitting diode (LED) as an indicator, enabling real-time as well as POC diagnosis of a prostate cancer marker. The proposed flexible MoS_2 FETs on a solution-based polyimide substrate show high-performance electrical properties as well as mechanical durability under various mechanical stress conditions. To quantitatively and directly characterize the physisorption of anti-PSA onto the surface of the MoS_2 channel, we employed Kelvin probe force microscopy (KPFM) for surface potential measurement and tapping-mode atomic force microscopy (tm-AFM) for tomographic analysis. Highly sensitive as well as real-time PSA detection down to 1 pg·mL^{-1}, which is far below the clinical

cut-off, was demonstrated under both normal and mechanically stressed conditions. Finally, inspiring system-level integration of the flexible MoS_2 FET biosensor, an epidermal skin-type biochip capable of detecting PSA in real time was fabricated.

2 Materials and methods

2.1 System overview

Figure 1 shows the overall architecture of an epidermal skin-type biochip and the mechanism of biosensing on the surface of MoS_2. Anti-PSA antibody is physically absorbed (i.e., physisorption) onto the MoS_2 channel without pre-surface chemical treatment attributed to the hydrophobicity of the MoS_2 surface, where the MoS_2 surface has a relatively high contact angle of ~75.77°. A PSA is specifically bound to the antibody, resulting in a conventional label-free immunoassay. Because most proteins retain their ionized state corresponding to the pH of the aqueous solution during the lyophilization process [24, 25], the anti-PSA provides electric charges on the surface of MoS_2 and thus affects the channel conductance of the MoS_2 FET. Figure 1(c) shows a schematic diagram of the epidermal skin-type PSA biochip, and a photograph of the integrated biochip is shown in Fig. 1(d). The diagnostic part is composed of a commercial low-noise amplifier, differential comparator, and LED as an indicator of the diagnostic result; these were all integrated on a home-designed flexible printed circuit board (PCB). The sensing and diagnostic parts are connected through an anisotropic conductive film (ACF) bonding process.

2.2 Flexible MoS_2 FET fabrication

To fabricate the flexible bottom-gate multilayer MoS_2 FET as shown in Fig. 1(b), first, solution-type polyimide (PI) as a flexible substrate was spin-coated onto a glass substrate, followed by thermal annealing in a furnace at 350 °C. A Ti/Al (20 nm/50 nm) gate electrode was deposited using electron beam evaporation, and then, a hybrid gate dielectric of SU-8/Al_2O_3 was formed to enhance its mechanical flexibility and good adhesion of the metal on a flexible surface. An organic SU-8 (2000.5) layer (600 nm) was spin-coated and high-*k* Al_2O_3 (30 nm) was then deposited onto the SU-8 layer by atomic layer deposition (ALD). Afterward, MoS_2 flakes were mechanically exfoliated from bulk crystals

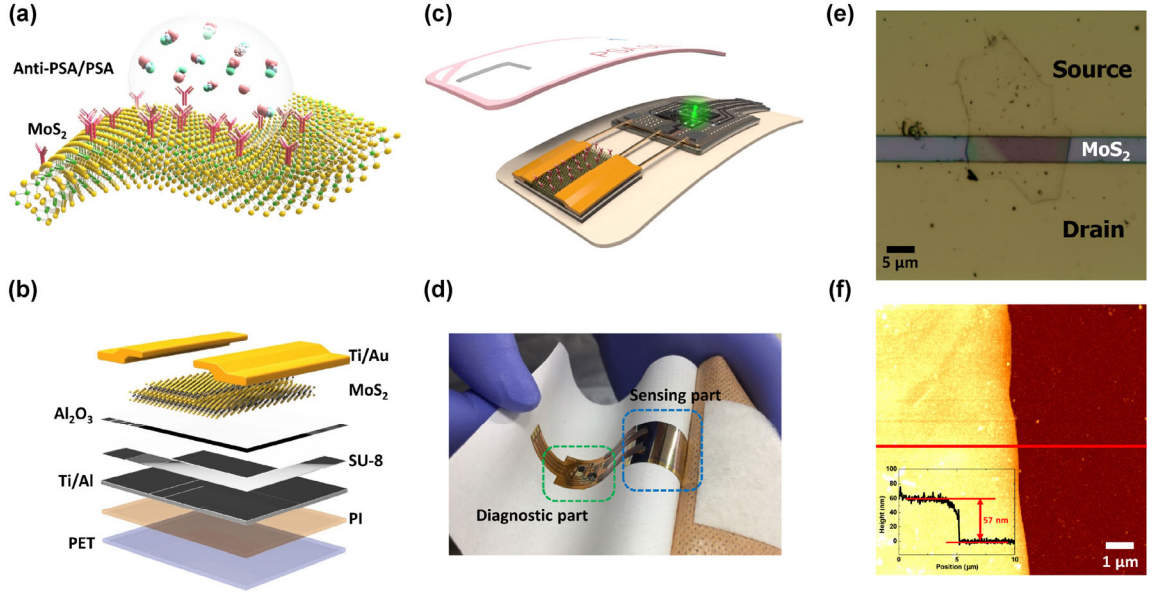

Figure 1 Illustration and demonstration of the platform of an epidermal skin-type MoS_2 biosensor system: (a) schematic of the flexible MoS_2 biosensor-detecting label-free immunoassay for PSA, where the PSA directly binds with the PSA antibody functionalized on the MoS_2 surface. (b) Schematic layout of the 2D multilayer MoS_2 FETs. (c) and (d) Schematic illustration (c) and photograph (d) of an epidermal skin-type MoS_2 biosensor system, consisting of the biosensor, read-out circuits, and LED as an indicator. (e) Optical image and (f) AFM image of a flexible MoS_2 device.

and transferred onto the substrate. For the source-drain (S/D) electrodes, Ti/Au (20 nm/100 nm) was deposited by e-beam evaporation, and patterned by conventional photolithography and wet etching. Post-thermal annealing was conducted at 150 ℃ for 2 h in a vacuum oven. Last, the thin PI film with the fabricated devices was separated from the glass by immersion in water, and a PET film (70 μm) was laminated beneath the PI substrate as a supportive layer. Figure 1(e) and 1(f) show an optical image and an AFM image of the fabricated MoS_2 device, respectively. The thickness of MoS_2 channel is about 57 nm.

2.3 Biological samples

A solution of 1 μg·mL^{-1} of anti-PSA antibody (Anti-h PSA 8311 SPRN-1, Medix Biochemica) in phosphate buffer saline (PBS, pH = 7.2) was dispensed and immobilized on the MoS_2 surface for 1 h in a humidity chamber. Then, the device was rinsed with PBS buffer for 1 min and dried for the measurements described in the following section. The anti-PSA-treated device was delivered and reacted with PSA (EMD millipore) in PBS for 10 min at room temperature, followed by rinsing with PBS for 1 min and drying to remove uncombined PSA. Four different concentrations of PSA solution (1 pg·mL^{-1}–1 ng·mL^{-1}) were tested sequentially.

2.4 Measurements

KPFM and tm-AFM were employed to characterize the physisorption of anti-PSA onto the MoS_2 channel by mapping the surface potential and to measure the surface morphology, respectively [26–28]. Pristine and antibody-treated MoS_2 surfaces were measured and analyzed. Electrical measurements were performed by using a semiconductor parameter analyzer (Keithley 4200-SCS) under atmospheric environment for the PSA concentrations of 1 pg·mL^{-1}–1 ng·mL^{-1}. For the static bending test, the fabricated devices were attached to rigid cylinders with various pre-defined radii of 10, 5, and 3 mm, and *I*–*V* measurements were performed. For the cyclic bending test, the number of bending cycles and radii were controlled using a multi-modal bending tester (Covotech Co., Ltd). Following the cyclic bending test, the electrical properties were investigated under the re-flat condition.

3 Results and discussion

3.1 Device characteristics of flexible MoS_2 FETs

Figure 2 shows the electrical properties of the fabricated MoS_2 FETs under normal and static/cyclic bending conditions. The thickness of the MoS_2 channel used in this work is distributed in the range of 66.5 ± 9.41 nm, as measured using AFM. From the measured transfer characteristics, the field-effect mobility (μ_{FE}) of 83.5 cm^2·V^{-1}·s^{-1} in a linear operation regime was extracted using

$$\mu_{FE} = \frac{g_m}{(W/L)\cdot C_{GI}\cdot V_{DS}}, \text{ and } g_m = \frac{\partial(I_{DS})}{\partial(V_{GS})} \quad (1)$$

where g_m = 1.24 × 10^{-6} S, W/L = 26.6 μm/8.3 μm, C_{GI} = 4.64 nF·cm^{-2}, and V_{DS} = 1 V. g_m is the transconductance, and C_{GI} is the total capacitance of the SU-8 (ε_r = 3.2) and Al_2O_3 (ε_r = 9.5) bilayer. The device exhibits an on/off-current ratio (I_{ON}/I_{OFF}) of ~10^6, and threshold voltage (V_{TH}) of –38.9 V, which was calculated using the linear extrapolation method at V_{DS} = 1 V. Note that the high performance of our devices is attributed to the SU-8 and Al_2O_3 bilayer hybrid gate insulator providing good interface properties as well as a long-range dielectric screening effect [29, 30].

To investigate the performance variations of our flexible MoS_2 FETs under mechanical stress, static and cyclic bending tests were performed with different bending radii and cycles, as shown in the inset of Figs. 2(a) and 2(b); *I*–*V* curves were measured for bending radii of 10, 5, and 3 mm and for bending cycles of 100, 1,000, 5,000 and 10,000. Figure 2(a) shows slight shifts of the transfer curves under flat, statically bent, and re-flat status. The variation of μ_{FE}, which was defined as ($\Delta\mu$ (%) = $|\mu_{bending} - \mu_{flat}|/\mu_{flat}$), for the different bending radii, was estimated to be <2.8%, and particularly, V_{TH} changed slightly or retained its initial value regardless of the bending radius (ΔV_{TH} < 4.1 V), as shown in Fig. 2(c). For the characteristics changes under cyclic bending, Fig. 2(b) exhibits no significant shift of transfer curves for various numbers of bending cycles. Both μ_{FE} and V_{TH} retained their initial values: $\Delta\mu$ < 2.7% and ΔV_{TH} ~ 3.5 V in Fig. 2(d). The obtained electrical performance with no apparent

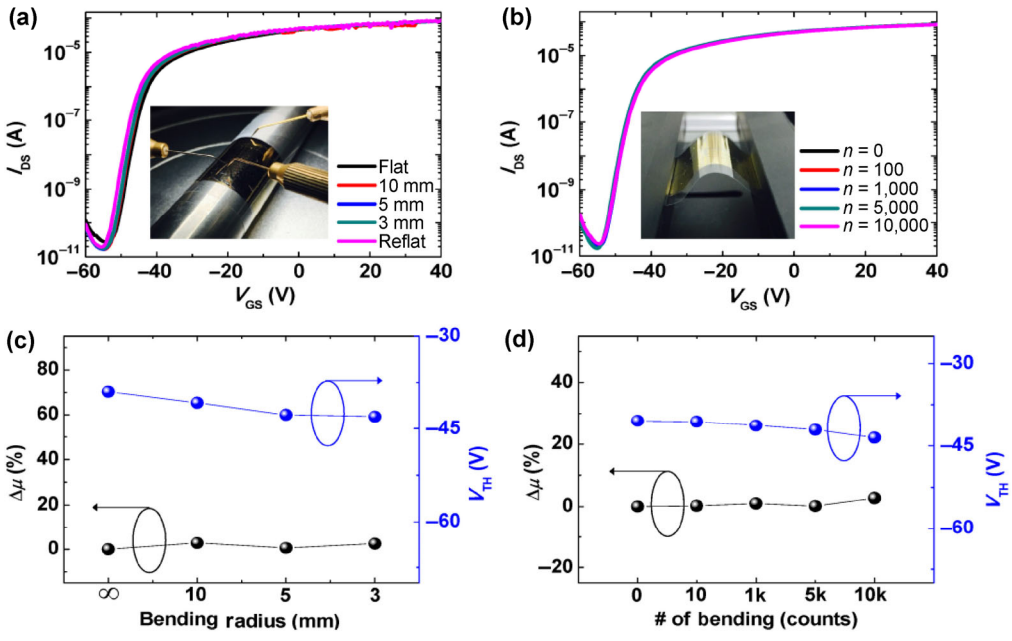

Figure 2 Electrical and mechanical characteristics of the flexible multilayer MoS_2 transistor under various mechanical stresses: (a) comparison of *I*–*V* characteristics of the flexible multilayer MoS_2 transistor under static bending conditions with four different bending radii (flat, r = 3, 5, and 10 mm). The inset shows a photograph of the bent devices attached on a rigid material. (b) Variation of the transfer characteristics under a cyclic bending test (r = 5 mm) with respect to bending cycles of 100, 1,000, 5,000, and 10,000. (c) and (d) Changes in μ_{FE} and V_{TH} with respect to static bending radii (c) and the number of bending cycles (d).

degradation under mechanical stress indicates that the flexible MoS_2 FETs could provide high mechanical flexibility, adapt to any curved surface, and function properly as a PSA biosensor regardless of its physical form, leading to portable and even wearable diagnostic applications.

3.2 Characterization of anti-PSA binding onto MoS_2 surface

The hydrophobicity of the MoS_2 surface provides higher affinity of biomolecules to the MoS_2 compared to other hydrophilic surfaces, and thus allows physisorption of the PSA antibodies onto the MoS_2 channel with no additional surface treatment, as illustrated in Fig. 3(a). In order to confirm the binding of anti-PSA onto the as-fabricated MoS_2 FET, we performed tm-AFM measurement to characterize the surface morphology, and used KPFM as a noninvasive method to obtain the electrostatic potential on the surface [31].

The tm-AFM topography images and KPFM surface potential maps of the channel before and after antibody treatment for a 1 μg·mL^{-1} concentration are shown in Fig. 3(b) and 3(c), respectively. The height of the antibodies obtained by tm-AFM prior to KPFM is distributed within 2.39 ± 0.55 nm. Compared with the neutral potential of the pristine MoS_2 surface (left), the positive potential was measured after antibody treatment (right) because the isoelectric point (pI) of anti-PSA (pI = ~7.8) resulted in net positive charges in the PBS (pH = ~7.2). Figure 3(d) shows the surface potential profiles along the horizontal axis in detail, and Fig. 3(e) shows the statistical distribution obtained from the areal KPFM measurement on the antibody-treated MoS_2 surface. The surface potential of pristine MoS_2 was measured as 1.57 ± 1.1 mV, and the physisorption of anti-PSA significantly increased the surface potential to 213.5 ± 25.3 mV. The inset of Fig. 3(e) shows the Gaussian-distributed surface potential histogram. The results obtained by performing tm-AFM and KPFM measurements on both pristine and anti-PSA-treated MoS_2 surfaces confirm that, without a specific surface treatment, the anti-PSA of 1 μg·mL^{-1} could be directly immobilized onto the MoS_2 surface without agglomeration.

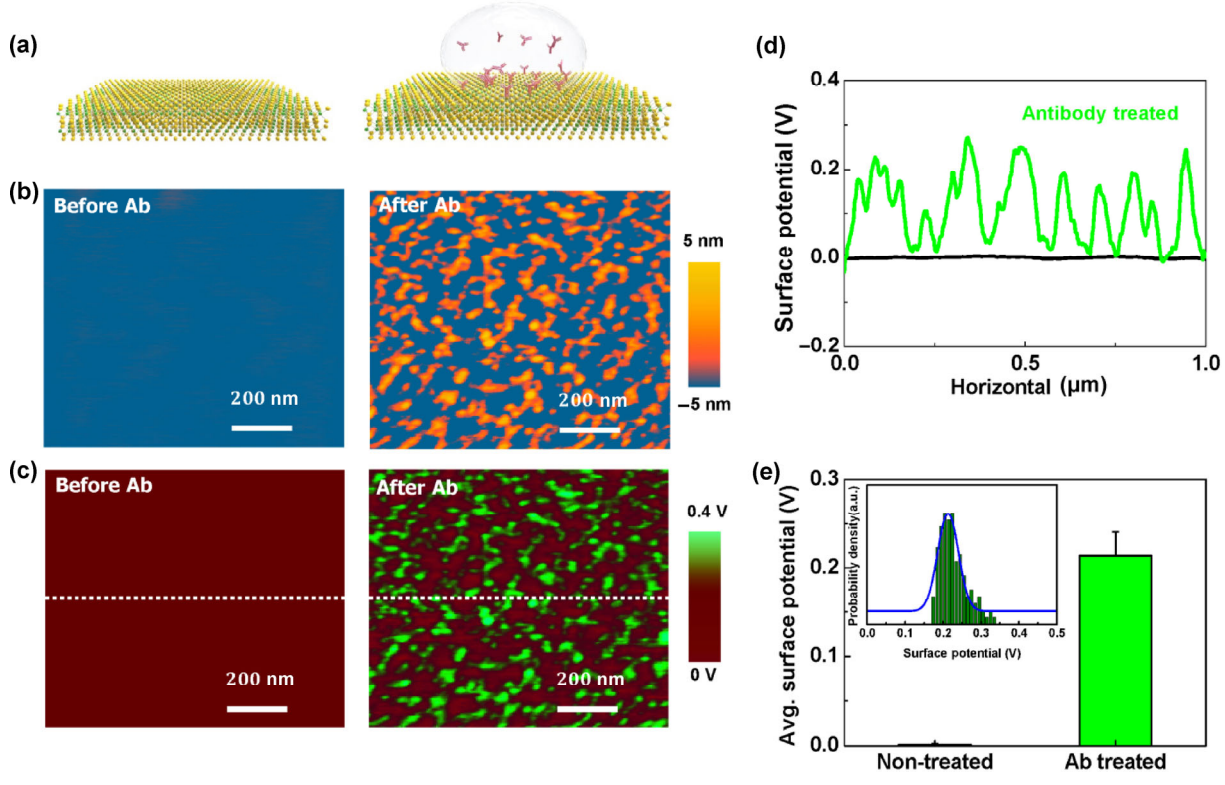

Figure 3 Mapping the surface potential of PSA antibodies on the MoS_2 surface using KPFM: (a) anti-PSA binding process on the MoS_2 surface. (b) and (c) Tapping-mode AFM images (b) and surface potential (KPFM) images (c) of the sample before and after anti-PSA treatment (1 μg·mL^{-1}). (d) Green and black lines represent the height of the surface potential along white dotted lines in (c). (e) Surface potential difference due to positively charged anti-PSA, (inset) surface potential distribution of antibody.

3.3 PSA detection of the flexible biochip based on MoS_2 FET

We then investigated PSA detection in the anti-PSA functionalized MoS_2 FET biosensor through electrostatically modulated off-current levels. Figures 4(a) and 4(b) represent the change of the transfer curves in response to the anti-PSA (1 μg·mL^{-1}) and four different concentrations of PSA solution (1, 10, 100, and 1,000 pg·mL^{-1}) under normal and static mechanical stress, respectively, with a bending radius of 10 mm. As the PSA concentration increases from 1 pg·mL^{-1} to 1 ng·mL^{-1}, the off-current at approximately V_{GS} = −35 V gradually decreases from ~5 nA to ~100 pA. When the positively charged anti-PSA biomolecules as confirmed by KPFM measurements bind to the surface of the MoS_2 channel, more electrons are accumulated during the off-state, and therefore, the off-current level increases significantly (~2 orders of magnitude). However, as the negatively charged PSA selectively binds to the immobilized antibody on the MoS_2 channel, the electrostatic effect caused by binding of the anti-PSA is reduced, and thus the off-current level (i.e., accumulated charges in the off-state) decreases.

Figures 4(c) and 4(d) show the changes of the off-current levels at V_{GS} = −35 V and V_{DS} = 1 V along the delivery of four different PSA concentrations (1 pg·mL^{-1} to 1 ng·mL^{-1}), presented under normal and static mechanical stress, respectively. Although the lowest detectable concentration of the devices was not tested, the detected concentration (1 pg·mL^{-1}) of PSA was already several orders of magnitude below the clinical cut-off level of 4 ng·mL^{-1}, demonstrating excellent sensitivity of the fabricated MoS_2 FET biosensor. Such a highly sensitive modulation is attributed to the nature of 2-D materials with a moderate band-gap [18, 20, 21]. A 2-D layered structure with high surface-to-volume ratio as well as pristine interfaces (i.e., in-plane dangling bonds) enable excellent electrostatic modulation. At the same time,

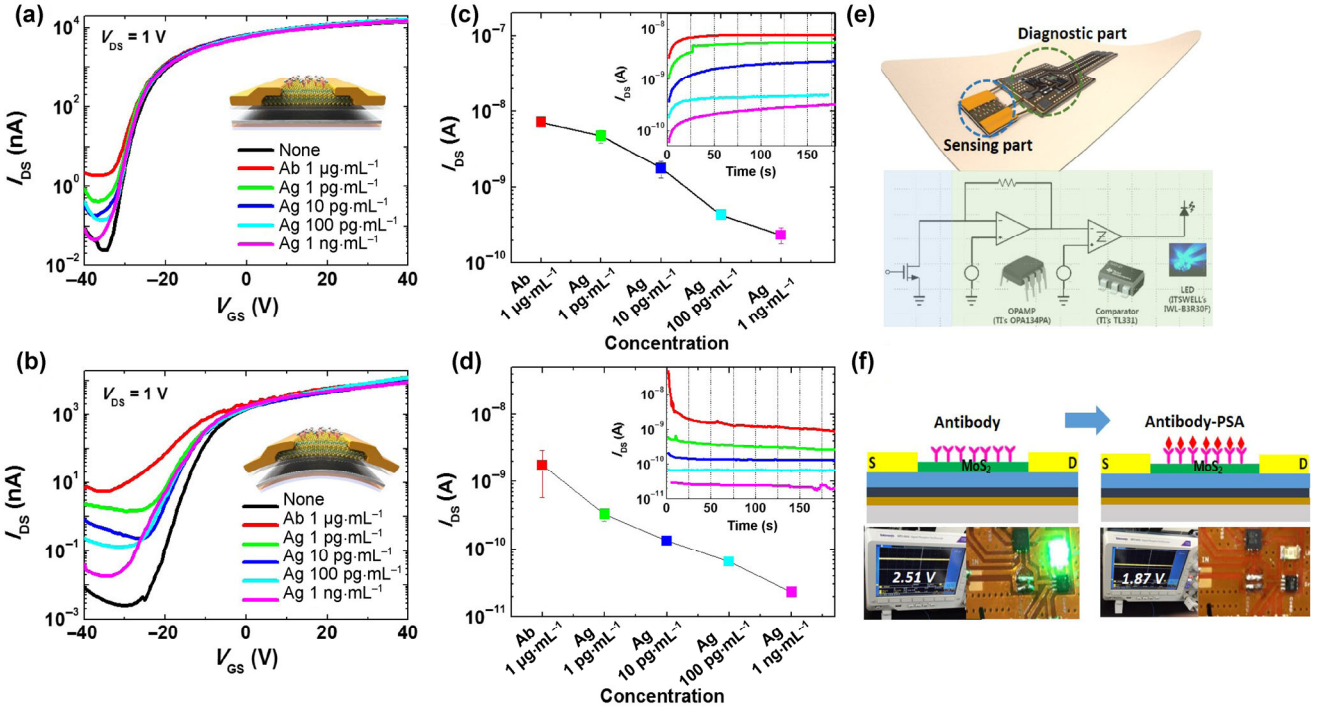

Figure 4 Epidermal skin-type MoS_2 biosensor and its sensing characteristics for PSA detection. (a) and (b) Transfer characteristics of our MoS_2 transistor biosensor with no bending stress (a) and 10-mm bending condition (b) with respect to various concentrations of PSA after the MoS_2 surface is functionalized by anti-PSA of 1 μg·mL^{-1}. (c) and (d) Real-time monitoring of the off-current versus various PSA concentrations with no bending stress (c) and 10-mm bending stress (d). Insets of (c) and (d) show the stabilized off-current level over a critical time at each PSA concentration. (e) Schematic feature of our flexible biochip and the read-out circuits. (f) Optical images of the LED indicator of the biochip for PSA detection, where the LED turns on after anti-PSA (μg·mL^{-1}) treatment, but PSA detection leads to turning it off.

the band-gap of multilayer MoS_2 (1.2 eV) suppresses leakage current while the MoS_2 FET is in the off-state. Therefore, surrounding net charges induced by the binding events at the interface between the biomolecules and MoS_2 can easily and efficiently modulate the off-current in the 2-D layered MoS_2 channel.

We further investigated the sensor's stability by off-current versus time measurements recorded for the PSA concentrations under both normal and static mechanical stressed conditions (bending radius, 10 mm). Although the sensor in the bent condition took relatively longer to stabilize with anti-PSA immobilization than that in the normal condition, both maintained the off-current level for 2–3 min. The obtained data demonstrated that our MoS_2 FET biosensors were stable as well as reliable enough to enable real-time detection of PSA regardless of their physical forms.

Finally, we performed a system-level integration of the flexible MoS_2 FET biosensor with read-out circuits and an LED on a home-made flexible PCB, and demonstrated an epidermal skin-type PSA biochip, as shown in Fig. 4(e). The read-out circuits consist of a transimpedance amplifier (TI, OPA134PA) amplifying the signal from the MoS_2 FET biosensor (i.e., off-current modulation induced by anti-PSA and PSA) to output voltage with a load resistance of 500 kΩ, which is read by a comparator (TI, TL331) to determine the signal level in comparison to a reference level and eventually, to drive the commercial green LED indicating a diagnostic result. An external battery powers the whole flexible biochip. Figure 4(f) shows the diagnostic results with schematic illustrations. When the anti-PSA of 1 μg·mL^{-1} was immobilized on the MoS_2 surface, the LED indicator turned on because of the increased off-current corresponding to the amplified output voltage of 2.51 V. Then, when the 100 pg·mL^{-1} PSA was delivered and bound to the immobilized antibodies

on the MoS_2, the off-current of the MoS_2 FET decreased, and so the output voltage decreased to 1.87 V, which is below the reference level of the comparator, and the LED turned off. The demonstrated results show that the proposed flexible PSA biochip can be used for detecting a prostate cancer marker as a POC diagnosis or near patients in daily life.

4 Conclusions

In summary, we have demonstrated a real-time electrical detection system, based on a flexible MoS_2 FET biosensor, for POC diagnosis of the prostate cancer marker. The fabricated MoS_2 FETs on a solution-based polyimide substrate exhibited high-performance electrical properties as well as mechanical durability during various bending tests. We characterized the surface potential and tomography using KPFM and tm-AFM, and the hydrophobicity of the MoS_2 surface enabled the physisorption of anti-PSA (~1 $\mu g \cdot mL^{-1}$) onto the MoS_2 channel without agglomeration. The immobilized MoS_2 FET biosensor can detect PSA concentrations as low as 1 $pg \cdot mL^{-1}$, which is several orders of magnitude lower than the clinical cut-off (~4 $ng \cdot mL^{-1}$), under normal and mechanically stressed conditions. Moreover, off-current modulation of the device due to immobilization of anti-PSA on the channel surface and specific binding of PSA was maintained for 2–3 min, providing a direct diagnostic result through the integrated read-out circuits and LED indicator. Further improvements, including multiplexed and highly sensitive analysis, can be achieved by fabricating a MoS_2 FET array incorporating distinct biomarkers and by integrating flexible OLEDs for a more portable and lightweight system. This highly sensitive, label-free, flexible, and simple PSA detection system based on a MoS_2-based FET biosensor not only enables POC diagnosis of prostate cancer, but also offers a great alternative to forensic service.

Acknowledgements

This research was supported in part by the National Research Foundation of Korea (Nos. NRF-2014M3A9D7070732, and NRF-2015R1A5A1037548). This research was supported by the Commercializations Promotion Agency for R&D Outcomes (COMPA) funded by the Ministry of Science, ICT and Future Planning (MISP).

References

[1] Özen, H.; Sözen, S. PSA isoforms in prostate cancer detection. *Eur. Urol. Suppl.* **2006**, *5*, 495–499.

[2] Barbosa, A. I.; Gehlot, P.; Sidapra, K.; Edwards, A. D.; Reis, N. M. Portable smartphone quantitation of prostate specific antigen (PSA) in a fluoropolymer microfluidic device. *Biosens. Bioelectron.* **2015**, *70*, 5–14.

[3] Taneja, S. S. Imaging in the diagnosis and management of prostate cancer. *Rev. Urol.* **2004**, *6*, 101–113.

[4] Raja, J.; Ramachandran, N.; Munneke, G.; Patel, U. Current status of transrectal ultrasound-guided prostate biopsy in the diagnosis of prostate cancer. *Clin. Radiol.* **2006**, *61*, 142–153.

[5] Hricak, H.; Choyke, P. L.; Eberhardt, S. C.; Leibel, S. A.; Scardino, P. T. Imaging prostate cancer: A multidisciplinary perspective. *Radiology* **2007**, *243*, 28–53.

[6] Yacoub, J. H.; Verma, S.; Moulton, J. S.; Eggener, S.; Oto, A. Imaging-guided prostate biopsy: Conventional and emerging techniques. *Radiographics* **2012**, *32*, 819–837.

[7] von Lode, P. Point-of-care immunotesting: Approaching the analytical performance of central laboratory methods. *Clin. Biochem.* **2005**, *38*, 591–606.

[8] Wang, J. Electrochemical biosensors: Towards point-of-care cancer diagnostics. *Biosens. Bioelectron.* **2006**, *21*, 1887–1892.

[9] Oh, S. W.; Kim, Y. M.; Kim, H. J.; Kim, S. J.; Cho, J. S.; Choi, E. Y. Point-of-care fluorescence immunoassay for prostate specific antigen. *Clin. Chim. Acta* **2009**, *406*, 18–22.

[10] Johnson, E. D.; Kotowski, T. M. Detection of prostate specific antigen by ELISA. *J. Forensic Sci.* **1993**, *38*, 250–258.

[11] Healy, D. A.; Hayes, C. J.; Leonard, P.; McKenna, L.; O'Kennedy, R. Biosensor developments: Application to prostate-specific antigen detection. *Trends Biotechnol.* **2007**, *25*, 125–131.

[12] Zheng, G. F.; Patolsky, F.; Cui, Y.; Wang, W. U.; Lieber, C. M. Multiplexed electrical detection of cancer markers with nanowire sensor arrays. *Nat. Biotechnol.* **2005**, *23*, 1294–1301.

[13] Cui, Y.; Wei, Q. Q.; Park, H.; Lieber, C. M. Nanowire nanosensors for highly sensitive and selective detection of biological and chemical species. *Science* **2001**, *293*, 1289–1292.

[14] Lee, K.; Nair, P. R.; Scott, A.; Alam, M. A.; Janes, D. B. Device considerations for development of conductance-based biosensors. *J. Appl. Phys.* **2009**, *105*, 102046.

[15] Yang, W. R.; Ratinac, K. R.; Ringer, S. P.; Thordarson, P.; Gooding, J. J.; Braet, F. Carbon nanomaterials in biosensors: Should you use nanotubes or graphene? *Angew. Chem., Int. Ed.* **2010**, *49*, 2114–2138.

[16] Kim, S.; Ju, S.; Back, J. H.; Xuan, Y.; Ye, P. D.; Shim, M.; Janes, D. B.; Mohammadi, S. Fully transparent thin-film transistors based on aligned carbon nanotube arrays and indium tin oxide electrodes. *Adv. Mater.* **2009**, *21*, 564–568.

[17] Kim, S.; Kim, S.; Park, J.; Ju, S.; Mohammadi, S. Fully transparent pixel circuits driven by random network carbon nanotube transistor circuitry. *ACS Nano* **2010**, *4*, 2994–2998.

[18] Sarkar, D.; Liu, W.; Xie, X. J.; Anselmo, A. C.; Mitragotri, S.; Banerjee, K. MoS_2 field-effect transistor for next-generation label-free biosensors. *ACS Nano.* **2014**, *8*, 3992–4003.

[19] Wang, L.; Wang, Y.; Wong, J. I.; Palacios, T.; Kong, J.; Yang, H. Y. Functionalized MoS_2 nanosheet-based field-effect biosensor for label-free sensitive detection of cancer marker proteins in solution. *Small* **2014**, *10*, 1101–1105.

[20] Lee, J.; Dak, P.; Lee, Y.; Park, H.; Choi, W.; Alam, M. A.; Kim, S. Two-dimensional layered MoS_2 biosensors enable highly sensitive detection of biomolecules. *Sci. Rep.* **2014**, *4*, 7352.

[21] Kalantar-Zadeh, K.; Ou, J. Z. Biosensors based on two-dimensional MoS_2. *ACS Sens.* **2016**, *1*, 5–16.

[22] Jung, C.; Kim, S. M.; Moon, H.; Han, G.; Kwon, J.; Hong, Y. K.; Omkaram, I.; Yoon, Y.; Kim, S.; Park, J. Highly crystalline CVD-grown multilayer $MoSe_2$ thin film transistor for fast photodetector. *Sci. Rep.* **2015**, *5*, 15313.

[23] Kim, S.; Konar, A.; Hwang, W.-S.; Lee, J. H.; Lee, J.; Yang, J.; Jung, C.; Kim, H.; Yoo, J.-B.; Choi, J.-Y. et al. High-mobility and low-power thin-film transistors based on multilayer MoS_2 crystals. *Nat. Commun.* **2012**, *3*, 1011.

[24] Costantino, H. R.; Griebenow, K.; Langer, R.; Klibanov, A. M. On the pH memory of lyophilized compounds containing protein functional groups. *Biotechnol. Bioeng.* **1997**, *53*, 345–348.

[25] Meyers, R. A. *Molecular Biology and Biotechnology: A Comprehensive Desk Reference*; Wiley-VCH: New York, 1995.

[26] Okamoto, K.; Yoshimoto, K.; Sugawara, Y.; Morita, S. KPFM imaging of Si(1 1 1)5 $\sqrt{3}$ ×5 $\sqrt{3}$ -Sb surface for atom distinction using NC-AFM. *Appl. Surf. Sci.* **2003**, *210*, 128–133.

[27] Liscio, A.; Palermo, V.; Samorì, P. Probing local surface potential of quasi-one-dimensional systems: A KPFM study of P3HT nanofibers. *Adv. Funct. Mater.* **2008**, *18*, 907–914.

[28] Bieletzki, M.; Hynninen, T.; Soini, T. M.; Pivetta, M.; Henry, C. R.; Foster, A. S.; Esch, F.; Barth, C.; Heiz, U. Topography and work function measurements of thin MgO(001) films on Ag(001) by Nc-AFM and KPFM. *Phys. Chem. Chem. Phys.* **2010**, *12*, 3203–3209.

[29] Bao, W. Z.; Cai, X. H.; Kim, D.; Sridhara, K.; Fuhrer, M. S. High mobility ambipolar MoS_2 field-effect transistors: Substrate and dielectric effects. *Appl. Phys. Lett.* **2013**, *102*, 42104.

[30] Song, W. G.; Kwon, H.-J.; Park, J.; Yeo, J.; Kim, M.; Park, S.; Yun, S.; Kyung, K.-U.; Grigoropoulos, C. P.; Kim, S. et al. High-performance flexible multilayer MoS_2 transistors on solution-based polyimide substrates. *Adv. Funct. Mater.* **2016**, *26*, 2426–2434.

[31] Hao, G. L.; Huang, Z. Y.; Liu, Y. D.; Qi, X.; Ren, L.; Peng, X. Y.; Yang, L. W.; Wei, X. L.; Zhong, J. X. Electrostatic properties of few-layer MoS_2 films. *AIP Adv.* **2013**, *3*, 42125.